INTER-ANNUAL VARIABILITY OF ACOUSTIC RAY TRAVEL TIMES IN THE NORTHEAST PACIFIC

by

John Alan Furgerson

B.S. Elect. Eng., University of Southern California (1987)

Submitted in partial fulfillment of the
requirements for the degree of

MASTER OF SCIENCE IN OCEAN ENGINEERING

at the

MASSACHUSETTS INSTITUTE OF TECHNOLOGY

and the

WOODS HOLE OCEANOGRAPHIC INSTITUTION

September 1990

INTER-ANNUAL VARIABILITY OF ACOUSTIC RAY TRAVEL TIMES IN THE NORTHEAST PACIFIC

by

John Alan Furgerson

Submitted to the Massachusetts Institute of Technology/
Woods Hole Oceanographic Institution
Joint Program in Oceanographic Engineering
on August 10, 1990, in partial fulfillment of the
requirements for the degree of
Master of Science in Ocean Engineering

Abstract

An acoustic tomography experiment consisting of a source near Hawaii and seven receivers along the west coast of North America was conducted from November 1987 to May 1988 and from February 1989 to July 1989. In this thesis, the acoustic ray travel times are analyzed in order to investigate inter-annual basin-scale thermal variability. These thermal fluctuations may help detect any greenhouse warming and greater understanding of them will increase knowledge of ocean-atmosphere interactions which affect weather and climate. A discussion of the program for finding the travel times is included along with a comparison of two methods of measuring travel times.

Thesis Supervisor: Dr. John L. Spiesberger
Woods Hole Oceanographic Institution

Acknowledgements

I would first off like to thank my thesis advisor, John Spiesberger, for his guidance and encouragement.

I am very appreciative of Betsy Pratt's work in preparing some of the figures for this thesis and of Marga McElroy , Bob Headrick, and Wayne Blanding for their help with computer programming and other aspects of my research.

I would like to thank the US Navy for allowing me to continue my education in the MIT/WHOI Joint Program.

Finally, I thank God, Bob Mould, and Julie Roberts for helping me get to this point.

Contents

List of Figures

List of Tables

Chapter 1

Introduction

1.1 Acoustic Tomography

Ocean acoustic tomography was first proposed as a means of measuring mesoscale (about 100 km) processes by Walter Munk and Carl Wunsch (1979). The technique involves measuring the acoustic travel times between a source and receiver and consequently, from these measurements, inferring the sound speed and currents in between the instruments. A 1981 acoustic tomography experiment (Cornuelle et al., 1982; 1985) successfully mapped a 300 km by 300 km area section near Bermuda for sound speed anomalies. A 1981 experiment (Spiesberger et al., 1983) measured Gulf Stream meanders.

Acoustic tomography exploits the sound speed properties of the ocean. The sound speed depends upon the salinity, pressure, and temperature. When a ray passes through an interface between waters of different properties it bend towards the minimum sound speed (see FIGURE 1-1) according to Snell's Law,

$$\frac{cos\theta_1}{c_1} = \frac{cos\theta_2}{c_2} = \frac{cos\theta_i}{c_i} = constant, \tag{1.1}$$

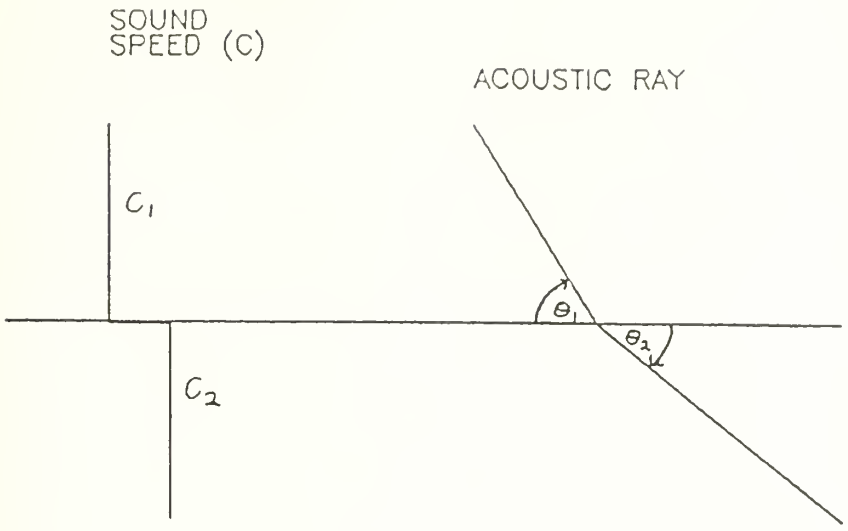

Figure 1-1: Ray traveling through interface and bending toward the smallest sound speed according to Snell's Law.

where θ_i is the angle the ray makes with the horizontal (grazing angle) and c_i is the sound speed in the layer.

In a typical mid-latitude portion of the ocean, the speed of sound decreases with distance from the surface due to a temperature drop. Below a certain depth, the temperature is relatively constant and the increase in pressure with depth causes the sound speed to increase. This forms an axis of minimum sound speed (sound channel axis) towards which the rays will be refracted. A sound speed profile for the Atlantic Ocean is given in FIGURE 1-2 (right side). The rays will constantly curve due to the changing sound speed. The paths of several rays are drawn in FIGURE 1-2 (left side) emanating from a source at a depth of 1.2 km. If a receiver were located on the sound channel axis 80 km away, only certain rays (called eigen-rays) would reach it. Rays which do not interact with the air-sea interface or the bottom will lose very little energy and can be detected at tremendous distances.

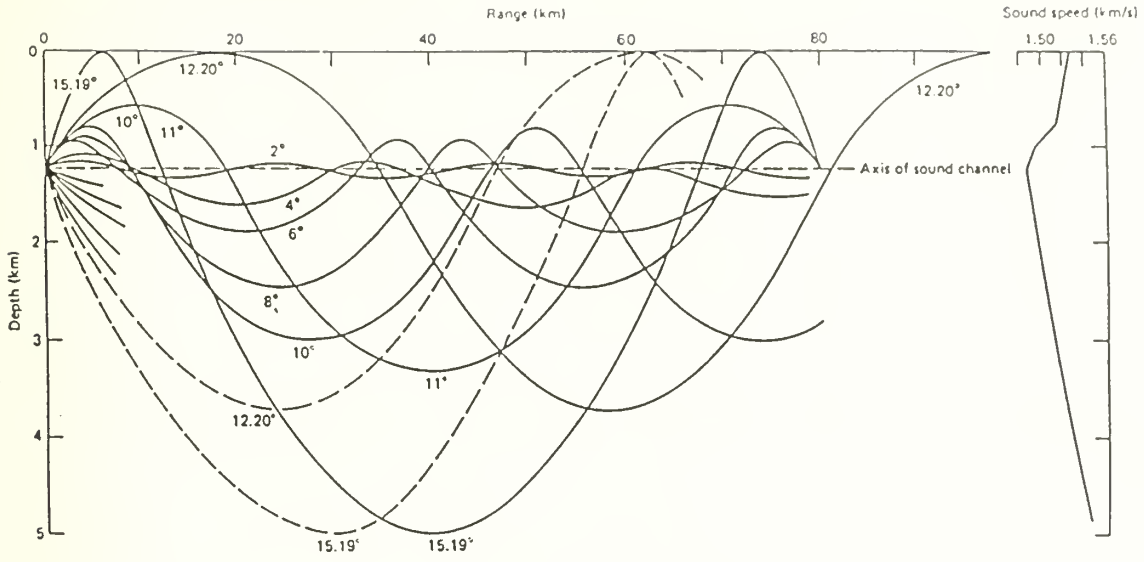

Figure 1-2: A typical sound speed profile is given on the right with some ray paths drawn on the left. Only certain rays, eigen-rays, will reach the receiver. (From Ewing and Worzel, 1948.)

The advantages acoustic tomography offers over traditional ocean observation techniques include:

1. As more sources (S) and receivers (R) are added to the tomographic array the amount of information increases by R $\times$ S instead of $R + S$ as with point measurements.

2. Acoustic tomography comes close to providing real time monitoring of the ocean since sound travels at approximately 1.5 km per second.

1.2 Motivation for Experiment

As human activities increase the carbon dioxide (CO_2) and other greenhouse gasses in the atmosphere, most climate models predict an increase in the earth's temperature due

to greenhouse warming. The temperature increase would not be felt uniformly across the globe (Stouffer et al., 1989). In 1983, Spiesberger began an acoustic tomography experiment for the primary purpose of monitoring global warming in the ocean (Spiesberger et al., 1990a,b).

A problem with the global climate models is the lack of knowledge of the ocean's role in affecting climate. The upper two and a half meters of the ocean has the same thermal capacity as the entire atmosphere (Gill, 1982) and fluxes of heat transported by the ocean and atmosphere are about equal (Vonder Haar and Oort, 1976). To confirm the accuracy of the models, a reliable method of measuring the ocean's temperature on the same spatial scale as the greenhouse warming model predictions is necessary (Barnett, 1990). The model of Stouffer et al. (1989) suggests a spatial structure on the order of 1000 to 10,000 km.

The usual method of determining the heat content of the ocean involves taking point measurements at hydrographic stations or by dropping expendable and air-expendable bathythermographs (XBT's and AXBT's). Point measurements of temperature are contaminated by variability on the meso ($\sim$ 100 km, $\sim$ 30 days) and fine ($\sim 10 - 1000$ m, $\sim 0.3 - 24$ hr) scales (Spiesberger et al., 1990a,b). Random and systematic errors are present (Hanawa and Yoritaka, 1987) along with nonuniformities between XBT's from different production runs (Wyrtki and Uhrich, 1982). Therefore, monthly average temperature anomalies cannot be measured from hydrographic data (Spiesberger et al., 1990a,b; Wyrtki and Uhrich, 1982).

Acoustic tomography is a powerful tool for monitoring large-scale variability (Spiesberger et al., 1990a,b). Using a few acoustic instruments, the large-scale thermal fluc-

tuations in the ocean can be measured which may improve understanding of the ocean's affect on weather, climate, ocean circulation, and greenhouse warming (Spiesberger et al., 1990a,b).

Chapter 2

The Experiment

The experiment used one source and seven receivers. The location of the equipment can be seen in FIGURE 2-1(upper left). The acoustic source was located on the Oahu slope off of Kaneohe Bay in 183 m of water and the receivers were bottom-mounted at differing ocean depths.

Source 1 (S1) transmitted to all seven receivers from 21 November 1987 to 9 May 1988. It was then repaired and redeployed approximately 20 m from its original position. It then functioned from 2 February 1989 to 5 July 1989 with a shutdown period of ten days centered around 18 April and one of five days around 3 May. The distance from S1 to the receivers ranged from 2000 to 4000 km. In general, data was obtained from all receivers during the period in which S1 transmitted except for short breaks due to power interruptions and data recording failures. No data is available in 1989 for R1 and R2.

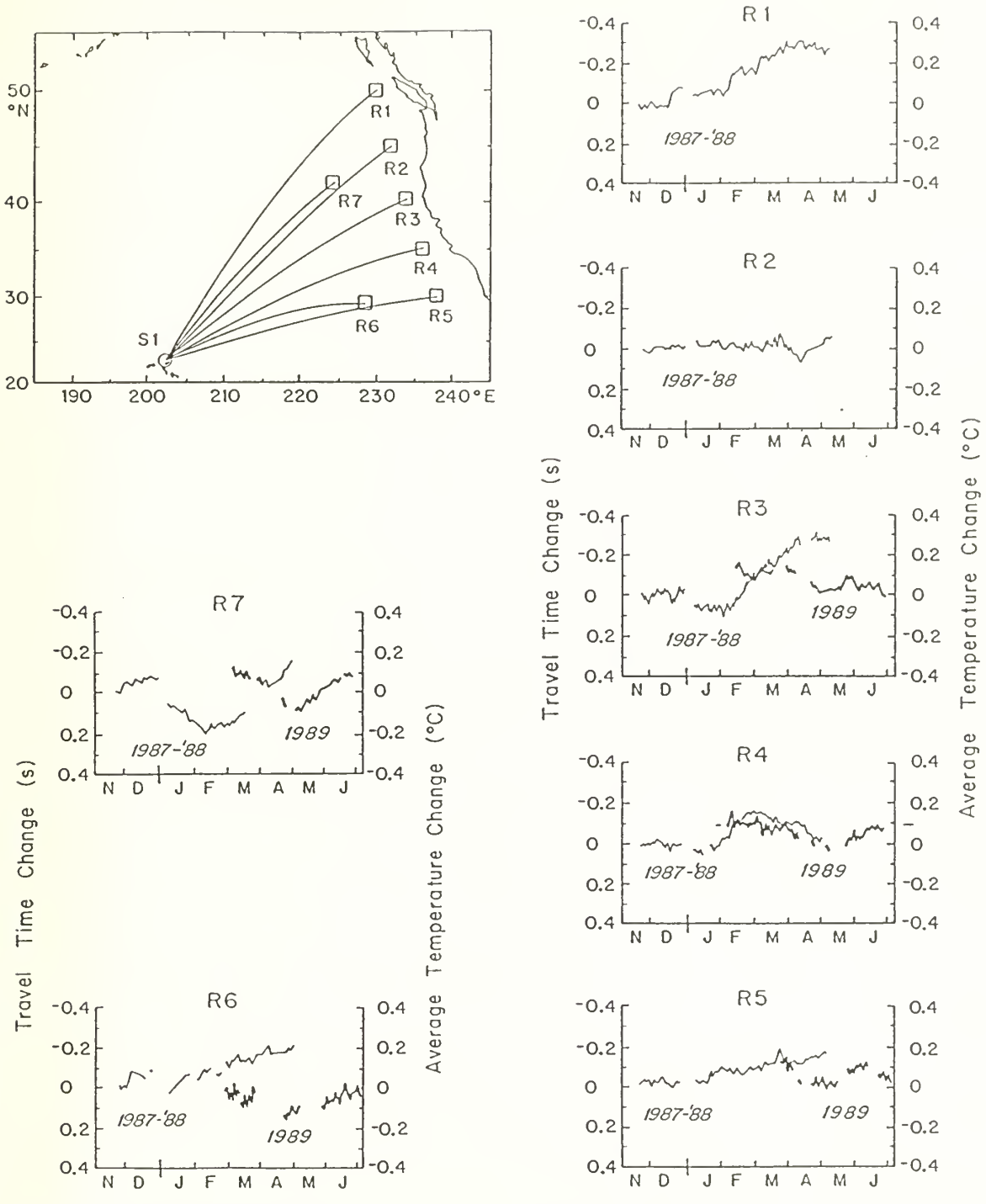

Figure 2-1: Map of the experiment (upper left) and the travel times at each source-receiver pair (SRP). Travel time changes (reckoned to the first 1987 datum) are on the left vertical axis and the approximate temperature changes are given on the right vertical axis. The thin lines are for 1987–88 data and the thick lines for 1989 data.

Chapter 3

Data Processing

3.1 Signal Processing

The signal generator for the source produces a pulse-like signal. The signal generator is located on land so that the signal must be amplified before travelling through a five mile length of cable to the acoustic source. The multi-path signal from S1 was recorded every 18 minutes so that there are about 76 records per day. The clocks for the signal generator and receivers are maintained by rubidium oscillators and a GOES satellite receiver.

Since the source cannot transmit a pulse powerful enough to be received above the background noise level, a phase-modulated signal is sent out instead. S1 used a 133 Hz carrier frequency phase-modulated every 8 cycles by a 255 digit linear maximal shift register sequence. Each digit has a length of $(8/133) \cong 60$ ms. The sequence has a period of $255(8/133) \cong 15.338$ s. By correlating the received signal with a replica, the energy in a 255 digit period is compressed into the 60 ms single digit period increasing the signal-to-noise ratio (SNR) by $10\log(255) \cong 24$ decibels (dB). Four consecutive periods

are coherently averaged to increase the SNR by $10 \log 4 \cong 6$ dB. Next, a running average of four complex samples gives another 6 dB gain for a total increase in SNR of about 36 dB (Metzger, 1983; Bushong, 1987; Spiesberger et al., 1989).

3.2 Stability of Signal

Adjacent individual amplitude records for yearday 153 1988 of Source 1 to Receiver 5 (S1R5) data are shown in Figure 3-1 (bottom). The adjacent records are not alike due to internal-wave induced sound speed fluctuations and interactions with the bottom (Spiesberger, personal communication). The incoherent averaging of records over a given day reduces the variability of waves with periods much less than the given period (Spiesberger et al., 1980). The incoherent average is defined by,

$$a[m] = [\frac{1}{N_{rec}} \sum_{r=1}^{N_{rec}} \|d[m,r]\|^2]^{1/2}, \tag{3.1}$$

where the m*th* complex demodulate of the r*th* record is d[m,r] and N_{rec} is the number of records being averaged (Spiesberger et al., 1989). The incoherent average of three adjacent records for hours one to six are given in FIGURE 3-1(top) and four hour incoherent averages of about 13 records each in FIGURE 3-2 (bottom).

Next are the daily ($\sim$ 76 record) incoherent averages for six consecutive days (FIGURE 3-2, top). The dashed lines indicate the six rays that are being tracked for this source-receiver pair (SRP). For most of the SRP's the daily averages were used to track the travel times of the rays. For S1R3, S1R4 and S1R7 1989 data, two day averages ($\sim$ 150 records) were used to increased the SNR at the expense of halving the amount of data. The final stability graph (FIGURE 3-3) for S1R5 data contains daily averages

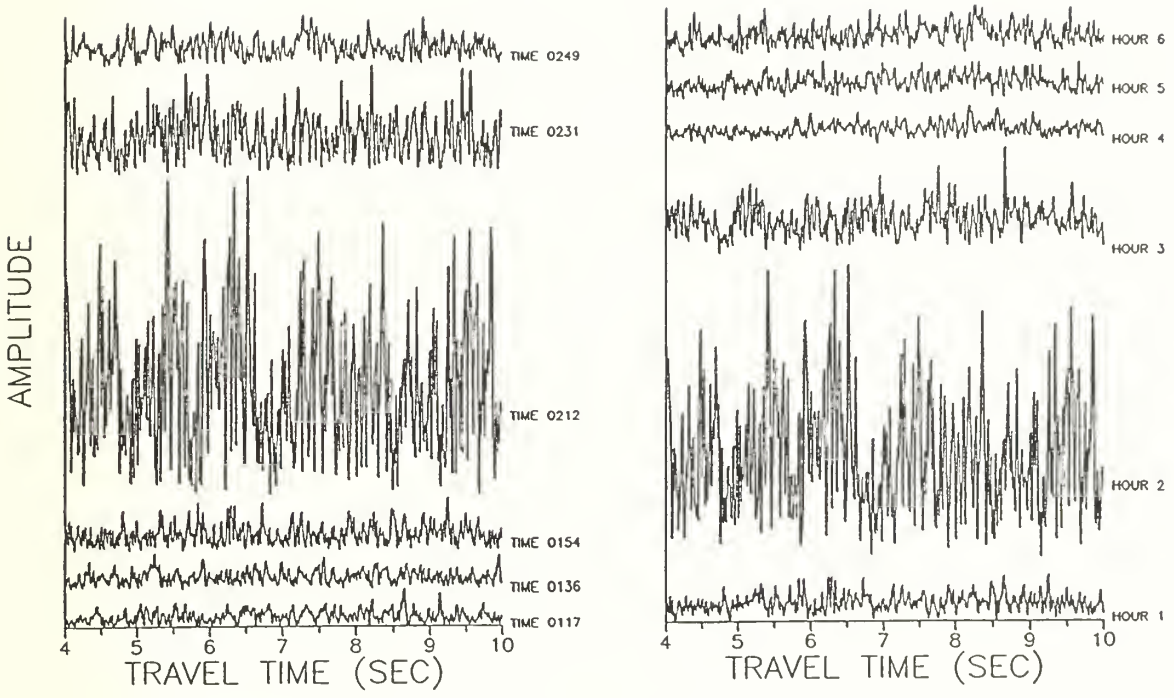

Figure 3-1: Six adjacent amplitude records (left) and six incoherently averaged hourly records (right), consisting of the three records which occurred in the hour, for S1R5 yearday 153 1988 data. The records show little resemblance to each other due to internal waves perturbing the sound speed field and bottom interactions. The background noise increases due to various surface phenomena including storms (effects last $\sim$ 3 days) and ships ($\sim$ 1 hour) (Spiesberger et al., 1980).

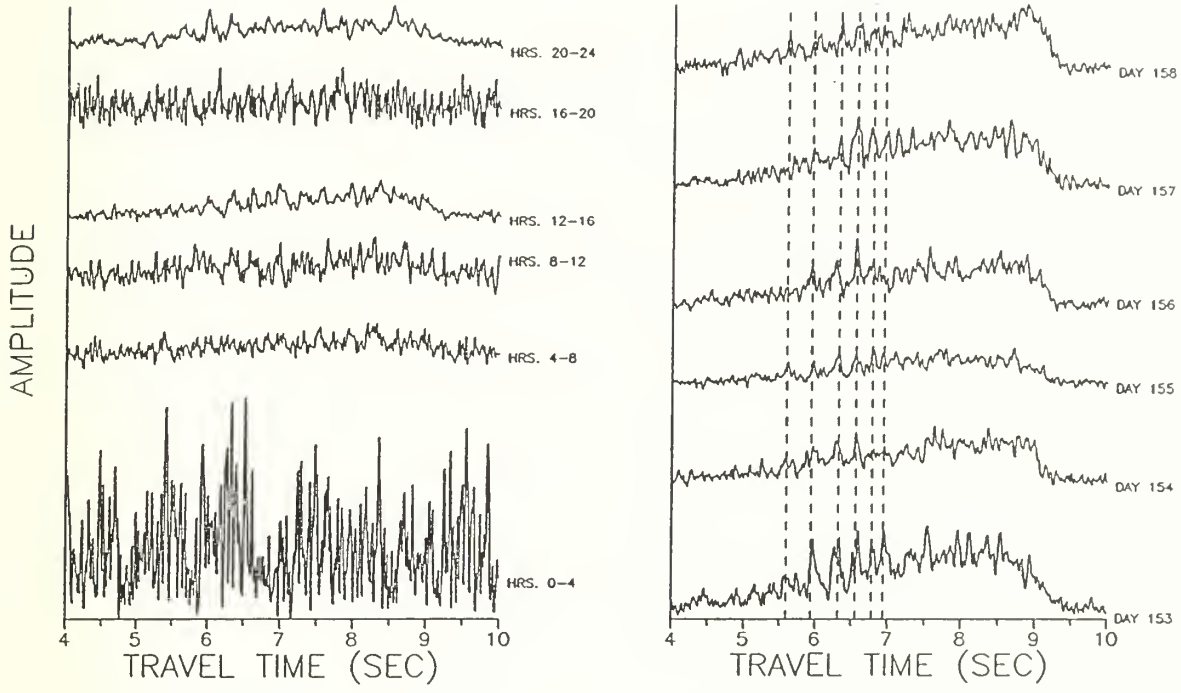

Figure 3-2: Four hour (left) and daily (right) incoherent averages consisting of about 13 and 76 records respectively for S1R5 1988 data. As the time length of the averages increase past the internal wave periods, the variability of the averages decreases. Dashed lines indicate stable arrivals.

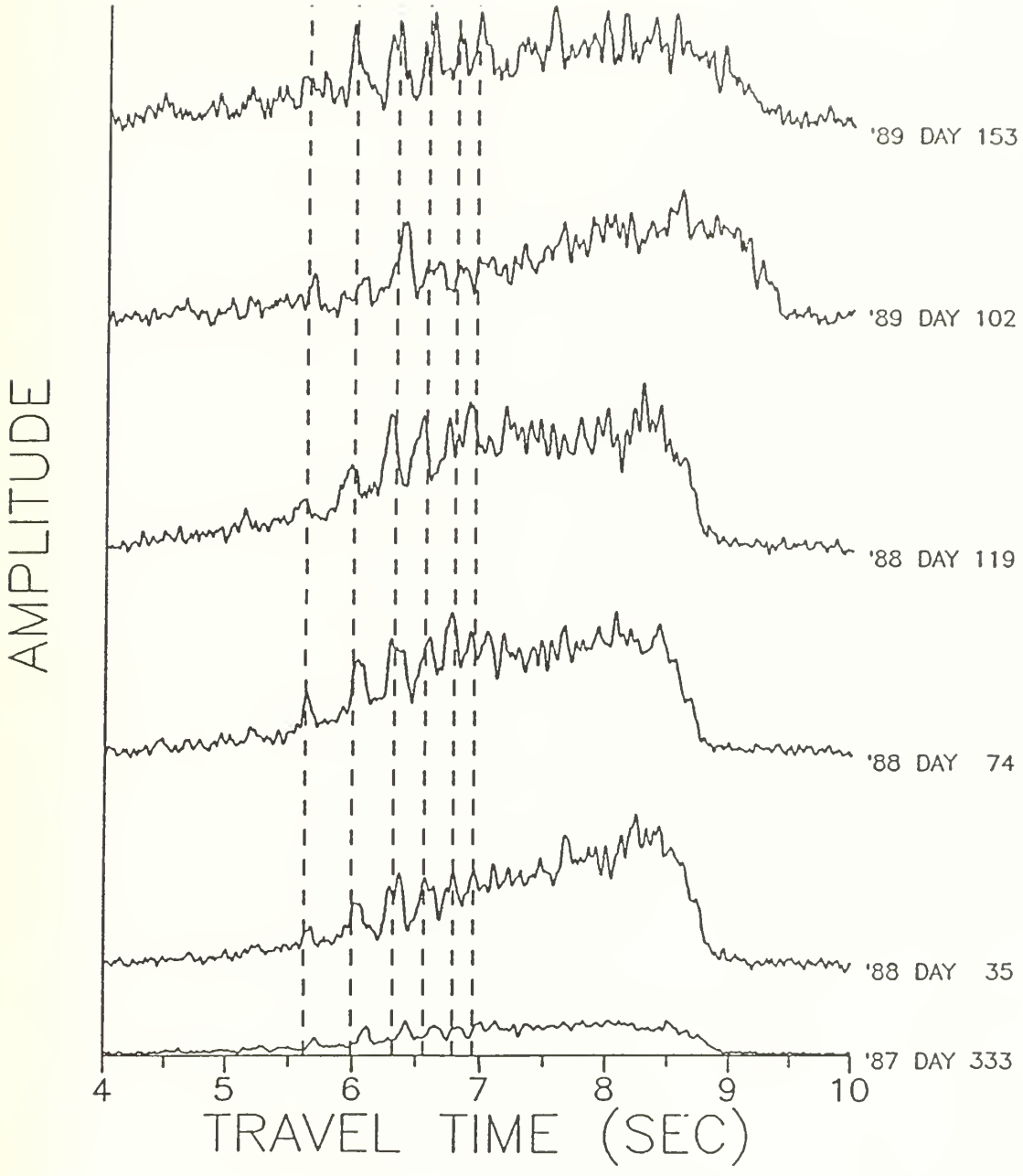

Figure 3-3: Daily averaged records from each of the three years of S1R5 data. Dashed lines are drawn to illustrate the stable arrivals.

for days in each of the three years. The daily averages exhibit stability over multi-year periods.

3.3 Ray Travel Time Measurement

A peak finding program, PCFIND, was used to measure the travel times of the acoustic rays. Some consider the peak amplitude to be the measure of a ray's arrival while others consider the centroid determined about the peak as the better measure. PCFIND will find both. It first finds the peaks in the incoherent average files. A window is then set up within which the average amplitude is determined. PCFIND slides this window around the peak in order to find the maximum average amplitude. Within this window the centroid is found. The travel times of the peaks and centroids are written to separate files. Details of PCFIND are in Appendix A. A comparison of peak and centroid data is in Appendix B.

3.4 Reduction of Data

The peak travel times for S1R3 are graphed in Figure 3-4 including 1983 data from a previous experiment. To the first order, the travel time changes are the same and therefore the changes were averaged for each day. First, the ray with the highest number of "good" data points was chosen as the reference ray. Then the average offset of the other rays from this reference ray is determined by,

$$T_{off_c} = \frac{1}{N} \sum_{i=1}^{N} T_{ic} - T_{ir}, \tag{3.2}$$

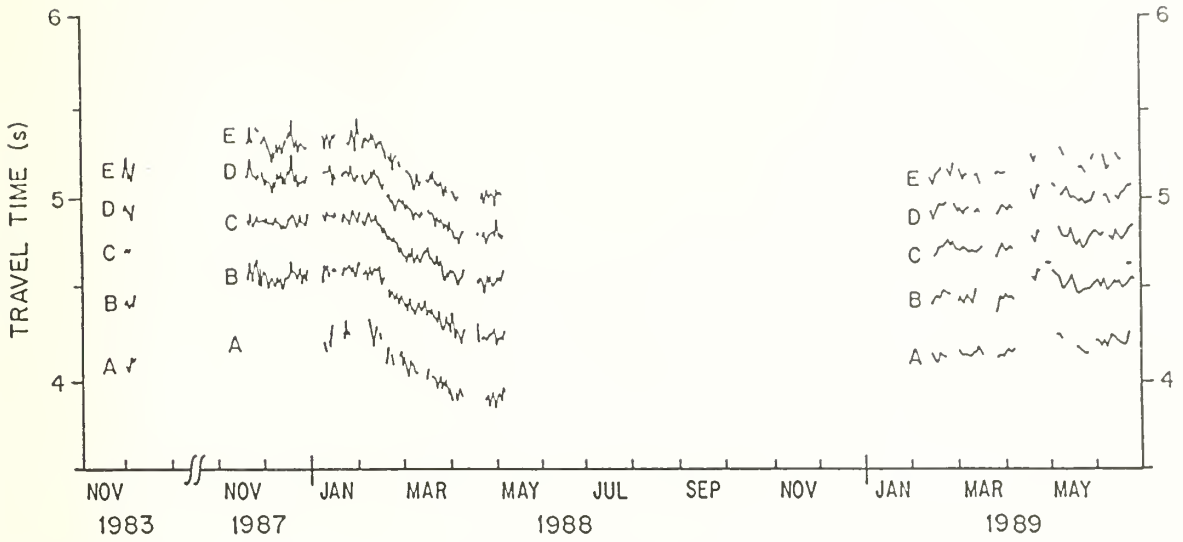

Figure 3-4: Peak travel times of the five rays tracked for S1R3 including 1983 data from a previous experiment. The long breaks in the data are due to source shutdowns. Small gaps are due to short term equipment breakdowns or an inability to track the rays. The travel times decrease in 1988 as the water begins to warm after a February cold peak. In 1989, the travel times increase from January to June indicating a temperature decrease.

where c refers to the particular ray, r is the reference ray, N is the number of common data points between rays c and r, and T is travel time reckoned to an arbitrary zero. The average travel time for each day j is then found from,

$$T_{ave_j} = \frac{1}{NRAYS - 1} \sum_{c=1}^{NRAYS} T_{cj} - T_{off_c}, \quad c \neq r, \tag{3.3}$$

where NRAYS is the number of tracked rays. The standard deviations of the offsets were also obtained.

Chapter 4

Results and Conclusions

4.1 Travel Times for Each Source-Receiver Pair

The collected data for each receiver is depicted in Figure 2-1. In the upper left corner of the figure is a map of the experiment.

For 1987–88 data, receivers R3, R6, and R7 show a similar signal. The waters cool in the winter, increasing the travel times, and begin to warm in the spring, decreasing the travel times. R1 and R5 in 1987–88 display some of the warming trend but none of the cooling in the winter. The travel times of R2 change very little. The signal for R4 is quite different from the others. A slight cooling trend is seen in to June 1988 when the water temperature begins to increase. In the beginning of March, however, a cooling trend begins which lasts until the data ends in late April.

All of the 1989 data starts with a cooling trend lasting in to April followed by a warming trend. The 1989 temperatures become cooler than the 1988 data in February or March for the SRP's where the plots cross. R3 shows no clear trend after mid-April. R5

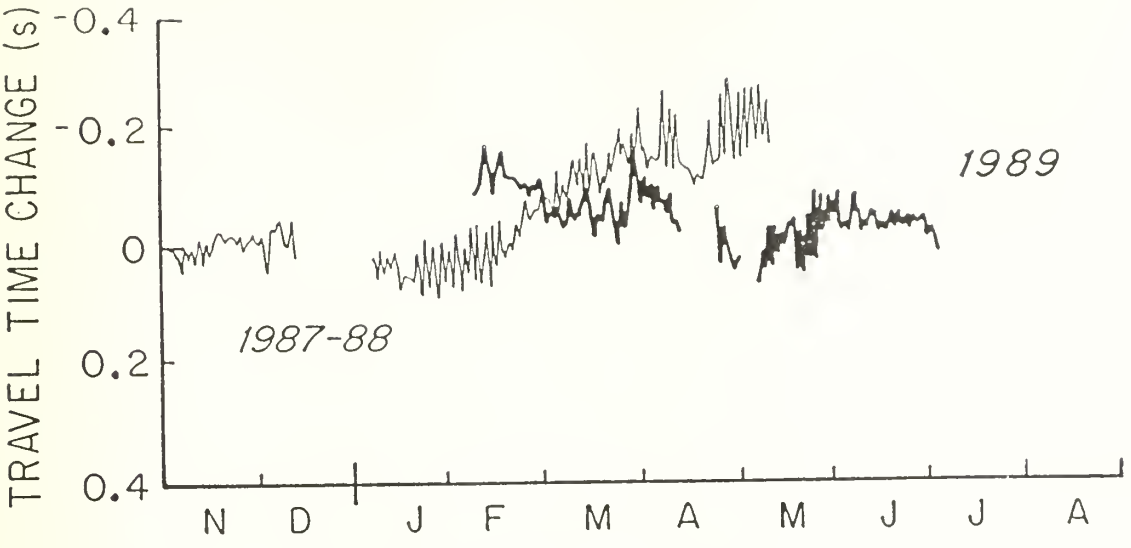

Figure 4-1: Spatial average of all SRP's

displays a cooling trend in late June.

A spatial average of the travel times of all SRP's is shown in FIGURE 4-1. The graph indicates a slight temperature decrease from November 1987 to the end of January 1988. The northeast Pacific then warms from February to May 1988. As the 1989 data begins, the waters are warmer in February than they were one year earlier. A cooling trend lasts from February to April 1989 followed by a slight warming trend. The overall result for the northeast Pacific basin in 1989 is cooler water temperatures in June than in February.

4.2 Sea Surface Temperature Data

The travel time data are compared to the sea surface temperature (SST) monthly means from the *Oceanographic Monthly Summaries* (1987– 1989). The data from the *Oceanographic Monthly Summaries* is a blend of *in situ* data used to establish "benchmark" temperature values and satellite data used to determine the shape of the contour lines

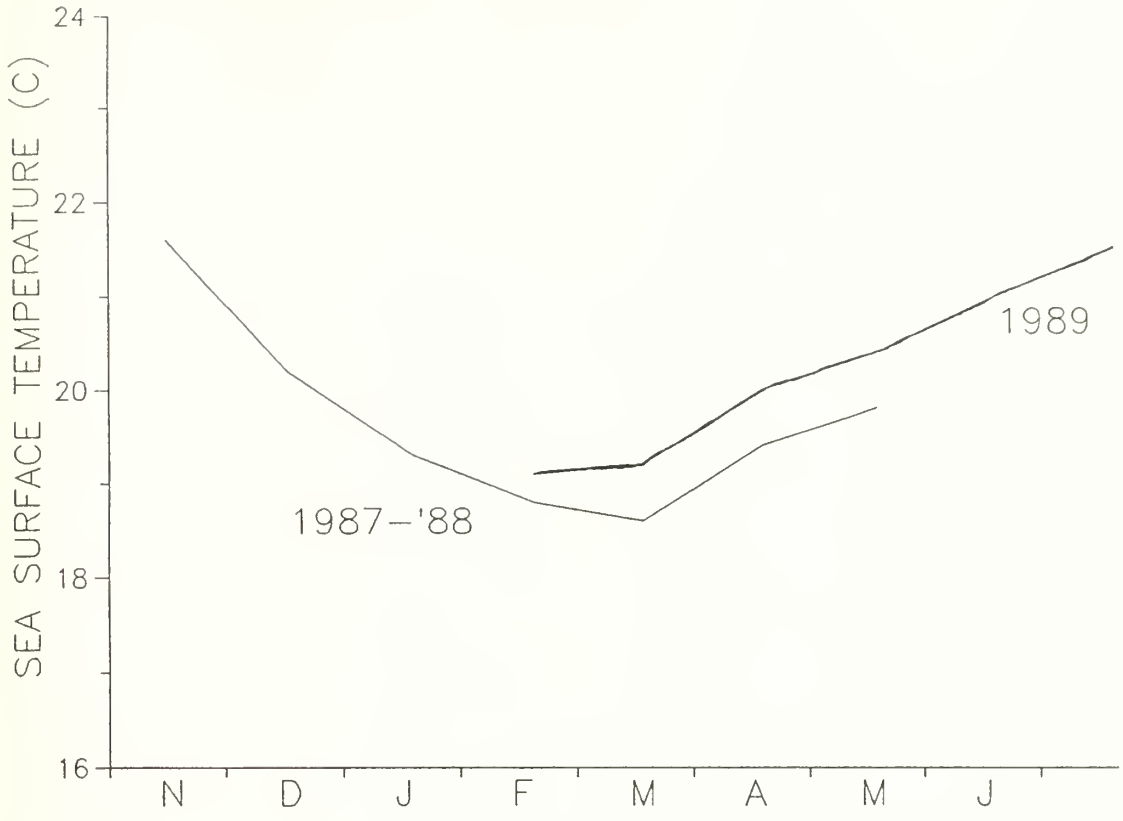

Figure 4-2: Monthly sea surface temperature average for the great circle path between Source 1 and Receiver 5.

between the points. The *in situ* data gives the bulk temperature of the top layer of water (on the order of meters) while the satellite data is indicative of the skin temperature of the top millimeter of water (Reynolds, 1988). The satellite data must be adjusted so that it coincides with the *in situ* data.

A monthly mean SST temperature between the source and a particular receiver was obtained by integrating along the great circle path. The spatially averaged monthly SST mean for S1R5 is plotted in Figure 4-2 and is to be compared with the travel time data in Figure 2-1. No correlation was observed for S1R5 nor for any of the other SRP's.

Since the acoustic rays sample a wider portion of the water column than the SST data,

they average the temperature of a greater volume of water. The tomographic data is also less dependent on seasonal temperature fluctuations and therefore makes a better measure of the inter-annual changes in heat content of the oceans (Spiesberger et al., 1990a,b).

4.3 El Niño Effects

Acoustic tomography can provide extensive temperature maps of the oceans which may provide a better understanding of events which affect weather and climate such as Los Niños. The term El Niño originally referred to the anomalous warming along the Peruvian coast which starts each year around Christmas. El Niño currently refers to anomalous warming centered along the equator in the central and eastern Pacific as part of an El Niño–Southern Oscillation (ENSO) event. Normally, the high temperatures in the central and eastern equatorial Pacific last for 10–15 months and are followed by an anomalous cold period named La Niña (Philander, 1990). Usually, Los Niños occur at 3–4 year intervals with stronger events at least 6–7 years apart (Enfield, 1989). Through atmospheric and ocean teleconnections, Los Niños affect areas far removed from the equatorial Pacific (Quinn et al., 1987; Philander, 1990).

The effects of El Niño reach the northeast Pacific basin in two ways. The atmospheric link is provided by Hadley cells which circulate warm air rising along the equator to atmospheric downdrafts in the mid-latitudes. The ocean link takes the form of coastally-trapped Kelvin waves which move poleward at about 200 cm/s (Johnson and O'Brien, 1990). Trenberth (1989) credits the 1986–1987 El Niño as a major cause of the 1988 North American drought. The cooling of a La Niña also affects large-scale atmospheric

circulation (Bradley et al., 1987).

It is too early for any in-depth analysis of the northeast Pacific response to the 1986–87 El Niño. Studies of earlier Los Niños (Emery and Hamilton, 1985; Johnson and O'Brien, 1990) show that the response to events of equal intensity can be quite different. Emery and Hamilton show anomalous warming throughout the northeast Pacific nine months after the peak equatorial warming of the strong 1957–58 El Niño. But, nine months after the peak equatorial warming of the strong 1972–73 El Niño, there is anomalous cooling in a 900 km band along the entire North American coast and between 20° N and 30° N latitude (Emery and Hamilton, 1985). After the moderate intensity event in 1976–77, there were above normal temperatures throughout the tomographic area (Emery and Hamilton, 1985).

The El Niño of 1986–87 may have affected the acoustic travel times. This event was classified as moderate in intensity by Quinn et al. (1987). The eastern equatorial Pacific waters reached a peak of about 1.8°C above normal in August 1987 (Trenberth et al., 1988). Applying a nine month delay in the northeast Pacific response to the August 1987 peak warming, one would predict a warming or cooling peak during May 1988 in the northeast Pacific. The data (FIGURE 4-1) shows warming up to the predicted peak in May 1988. Future work is required to determine if the acoustic travel times are responding to the 1986–1987 El Niño including a comparison to hydrographic data.

On 16 February 1990, the National Weather Service's Climate Analysis Center released an ENSO advisory due to a rise in the SST in the central equatorial Pacific and a weakening of the equatorial trade winds (Monastersky, 1990). The placement of the receivers may be ideal for detecting a northward moving Kelvin wave. Receivers R6 and R7 should prove

useful in determining whether anomalous warming or cooling caused by the El Niño is restricted to a band along the coast or if it is basin-wide.

4.4 Conclusions

Acoustic tomography can measure the thermal properties of the ocean. The temperature data this experiment provides is uncorrelated with SST data obtained by standard methods. Since acoustic tomography averages the ocean's parameters over the entire source to receiver path, it is a better indication of the *in situ* heat content of the ocean than satellite data.

The averaging properties of acoustic tomography should prove useful in the measurement of any possible greenhouse warming. The northeast Pacific experiment shows the feasibility of detecting inter-annual basin-wide temperature changes in the ocean (Spiesberger et al., 1990a,b). To detect greenhouse warming, a tomographic system encompassing all of the world's oceans is needed.

The 1987–1989 experiment may indicate part of the northeast Pacific response to the 1986–1987 El Niño. Acoustic tomography may provide insight on the remote effects of an El Niño and in turn aid in the understanding of the inter-relationships between the atmosphere and oceans.

Appendix A

The Peak Finding Program

The records for a given SRP must be compared to each other visually to figure out how many rays are stable from day to day. The record with the most representative peak profile is chosen to be the replica. The intensity records are processed sequentially by the peak finding program, PCFIND.

The parameters which PCFIND asks for are as follows:

NAMEREP the name of the file to be used as the replica

NRAYS the number of rays to search for in each record

TMEST(NRAYS) the estimated travel time of each ray in the replica

SNRLIM $\pm$ the interval over which an average noise figure is determined

MINSNR the minimum signal-to-noise ratio of a peak to make it an acceptable data point

XCORDIS the positive or negative maximum lag allowed in the cross-correlation (used

to minimize computer processing time)

PKWIND the width of the peak search window

CENTWID width of the window for finding the maximum average intensity which is used to find the centroid

CENTDIS the distance to each side of the MAX PEAK that the centroid find window is slid in search of the maximum average intensity

The program first cross-correlates the replica with a given record. The resulting lag is added to the estimated ray travel times and a window of width PKWIND, centered at each of these adjusted times, is set up to search for the intensity peak for each ray. If the maximum intensity, called MAX PEAK, occurs at the edge of the window, it is compared to the next point over to ensure that it is of greater intensity and indeed a peak. Next, the average noise intensity is determined over the selected noise interval and the peak intensity is compared to it. If the SNR is less than the MINSNR or the MAX PEAK is not an actual peak, a negative number is recorded in an output file for the travel time instead of the actual time.

The location of the MAX PEAKS are the basis for finding the centroid travel times. A centroid search window is set up of width CENTWID. The center of this window slides a distance CENTDIS to each side of the MAX PEAK. At each data point that the center occupies the average intensity within the window is determined. The location of the centroid search window center where the maximum average intensity was found is used as the balance point in calculating the centroid within the window. These are called MAX CENTROIDS and are recorded in a separate file from the MAX PEAKS.

Another program filters out travel times for each ray which are unreasonably different in value from the other data for that ray. The program compares each ray's travel time to a running average of the previous five days of data for that ray. If the difference is greater than a chosen value (usually 80 msec), the data point is discarded.

Appendix B

Comparison of Peak and Centroid Data

The intensity record is corrupted by noise so that the exact arrival time of an acoustic ray is unknown. One method of tracking the arrivals is to assume that the time associated with the highest intensity peak is the travel time. Since the peaks are not fine lines, some consider the centroid about the maximum intensity to be the best estimate of the arrival time.

To show the difference between what PCFIND determines to be the MAX PEAK and the MAX CENTROID, the intensity record for day 213, hour 18 of S1R6 data is given in FIGURE B-1. In this figure, rays 2 and 8 are marked and shown in more detail in FIGURE B-2. The difference in peak and centroid travel times for ray 2 is 42 msec and for ray 8, 3 msec. The situation for ray 8 where the MAX CENTROID and PEAK essentially coincide is the usual one. For ray 2, there is more energy situated near 11.32 sec than

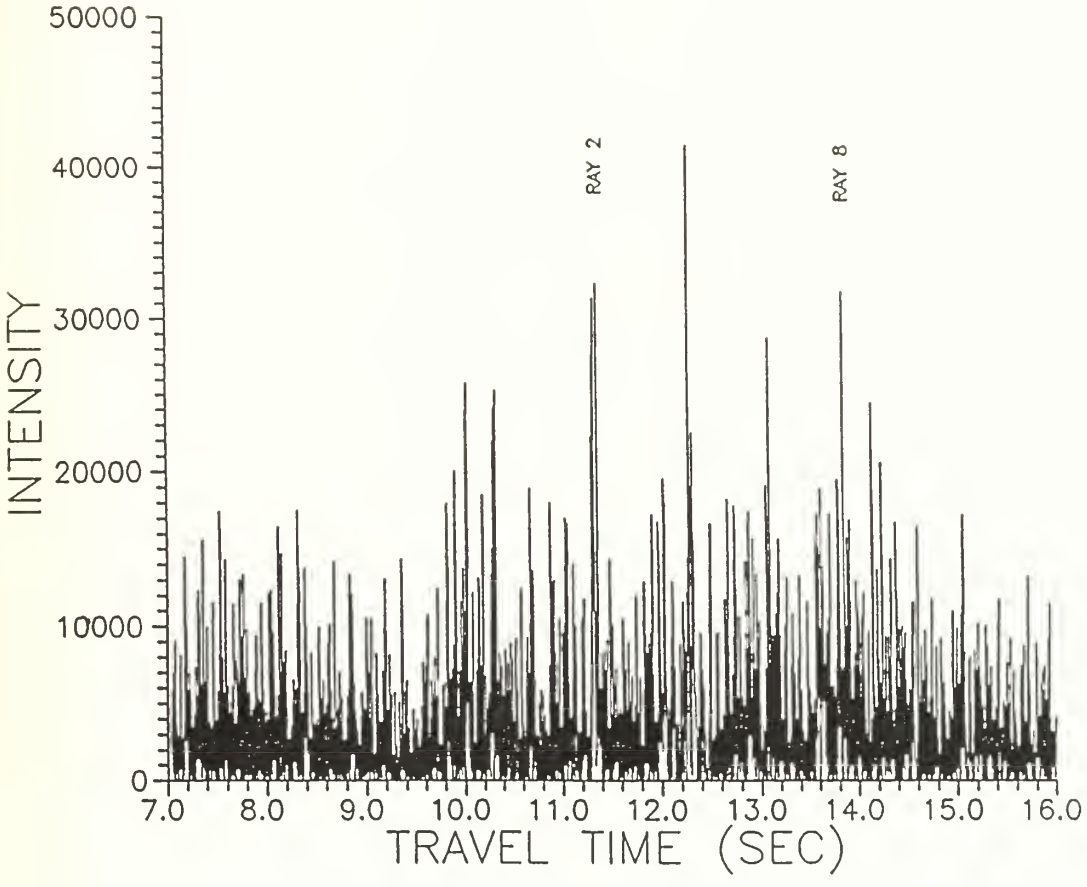

Figure B-1: Intensity Record for S1R6, day 213 of 1987, hour 18. Rays 2 and 8 will be examined to show how the peak finding program determines the peak and centroid travel times.

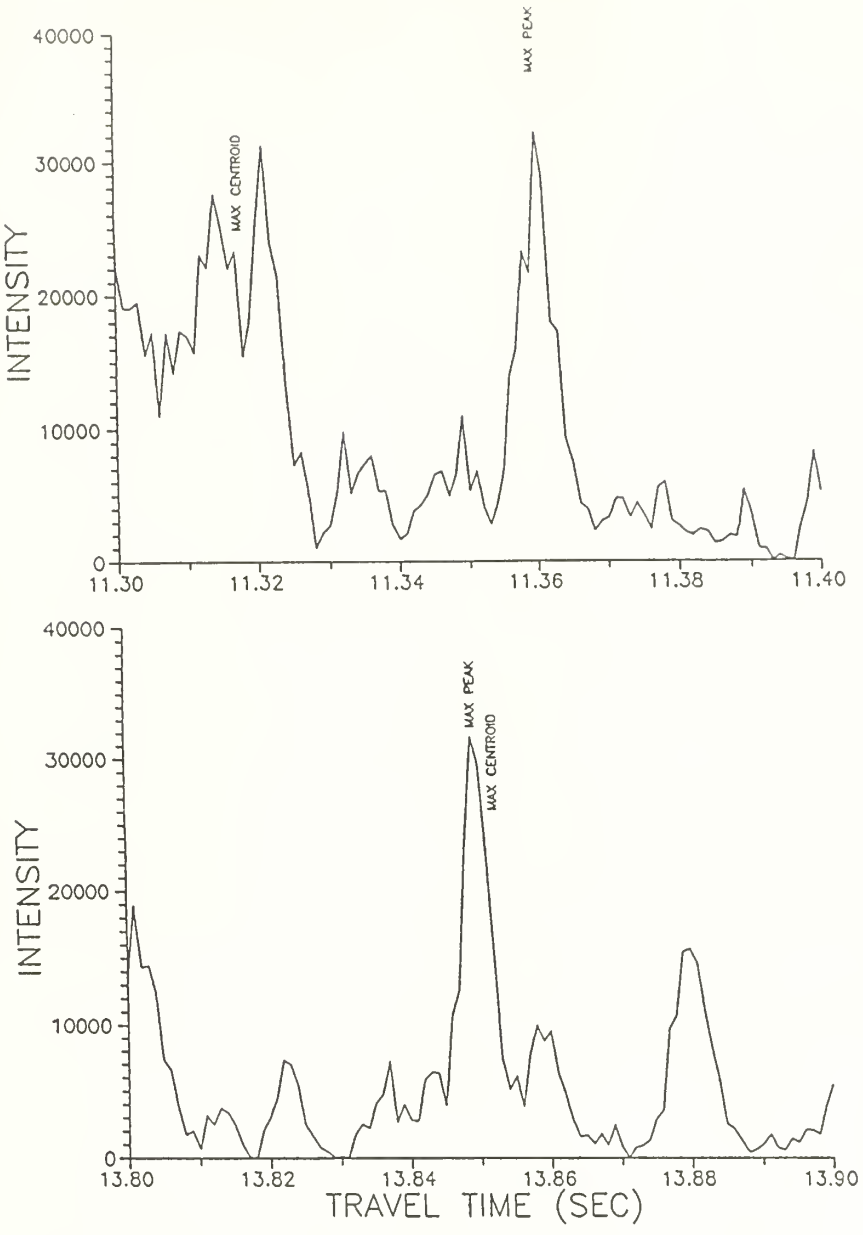

Figure B-2: In the top graph, the travel times are determined for ray 2. The program looks in the peak find window for the maximum intensity. This is found at about 11.360 seconds and is labelled MAX PEAK. Then a centroid find window is formed which slides along the time axis a distance called the centroid slide width on each side of MAX PEAK. Within this centroid find window, the average intensity is determined. The time location of the centroid find window middle with the maximum average intensity will be used as the balancing point in the determination of the centroid. The centroid of this maximum average intensity window is found at about 11.318 seconds and is labelled MAX CENTROID. In the bottom graph the travel times for ray 8 are shown. This is the more usual case where the MAX PEAK and MAX CENTROID are close together.

Type of Data	Number of Data	Average Travel Time (s)	Standard Deviation (ms)	Mean Standard Deviation (ms)
peak	7	11.312	32	12
centroid	7	11.308	26	10

Table B.1: Means and Standard Deviations of S1R6 Ray 2 1988 Yearday 213

Type of Data	Number of Data	Average Travel Time (s)	Standard Deviation (ms)	Mean Standard Deviation (ms)
peak	6	11.304	27	11
centroid	6	11.306	27	11

Table B.2: Means and Standard Deviations with Hour 18 Data Removed

11.36 sec so the MAX CENTROID is determined in the former area.

The centroid search window may have been allowed to slide too far from the MAX PEAK in finding the maximum average intensity. To find out, the means and standard deviations of ray 2 for yearday 213 must be examined (TABLE B.1). The third column represents the number of "good" travel time data points out of the twelve records for that day. The mean standard deviation is given by:

$$MSD = \sqrt{(\frac{SD^2}{NDATA})} \tag{B.1}$$

where:

MSD the mean standard deviation

SD the standard deviation

NDATA the number of "good" data points

TABLE B.2 then gives the mean and standard deviation for ray 2 with the hour 18 data removed. The MAX CENTROID time for yearday 213 hour 18 seems much more plausible than the MAX PEAK time when compared to the average travel times for ray 2 for that day. Additionally, the mean standard deviation decreases for the peak data

when hour 18 data is removed while the centroid mean standard deviation increases which shows that the centroid data is the better estimate and PCFIND did not conduct too wide of a search for the maximum average intensity.

Five days of S1R6 data were analyzed to decide if the MAX CENTROID or MAX PEAK data is the better estimator of the acoustic ray arrival times. The averages and standard deviations for the S1R6 data are shown in next three tables. TABLES B.3 and B.4 contain the MAX PEAK and MAX CENTROID data respectively and TABLE B.5 contains the same data for the time differences (MAX PEAK – MAX CENTROID). The standard deviations of the difference data are lower than the PEAK and CENTROID values which indicates that the two types of data attempt to measure the same parameter. The larger standard deviation values in TABLE B.5 indicate that for one of the particular ray travel time measurements for that day there was the situation where the MAX PEAK and CENTROID were far apart as in the previous hour 18 ray 2 data. The average of the mean standard deviation for the five days is 9.35 msec for the peak data and 8.95 msec for the centroid data. The centroid data would therefore be the better measure of travel time but only because of the 5.5% difference in mean standard deviations. Since only the trends in the travel time changes and not the absolute travel times are examined, MAX PEAK data has been used for all the graphs since it is easier to visualize the intensity peak as the mark of an acoustic ray's arrival.

YRDAY	RAY #	NUMBER OF DATA	AVG. TIME (S)	STANDARD DEVIATION (S)	MEAN STANDARD DEVIATION (S)
213	1	5	.1105660E+02	.1774933E-01	.7937743E-02
213	2	7	.1131157E+02	.3202157E-01	.1210302E-01
213	3	7	.1201800E+02	.1801585E-01	.6809351E-02
213	4	8	.1227337E+02	.1163990E-01	.4115327E-02
213	5	7	.1288514E+02	.3937890E-01	.1488382E-01
213	6	8	.1310812E+02	.3785970E-01	.1338543E-01
213	7	7	.1362486E+02	.2388316E-01	.9026988E-02
213	8	5	.1383760E+02	.2257069E-01	.1009392E-01
217	1	5	.1106160E+02	.1657228E-01	.7411350E-02
217	2	6	.1131633E+02	.1769807E-01	.7225205E-02
217	3	6	.1201683E+02	.1766732E-01	.7212652E-02
217	4	5	.1227740E+02	.2668786E-01	.1193517E-01
217	5	8	.1288337E+02	.2949956E-01	.1042967E-01
217	6	7	.1307471E+02	.3012197E-01	.1138504E-01
217	7	6	.1360650E+02	.2176961E-01	.8887408E-02
217	8	6	.1382467E+02	.1407929E-01	.5747848E-02
221	1	9	.1103733E+02	.1519518E-01	.5065060E-02
221	2	10	.1127800E+02	.2900353E-01	.9171725E-02
221	3	9	.1198700E+02	.3047766E-01	.1015922E-01
221	4	11	.1224364E+02	.2010084E-01	.6060630E-02
221	5	8	.1283950E+02	.2961860E-01	.1047176E-01
221	6	9	.1309033E+02	.2456738E-01	.8189127E-02
221	7	8	.1357887E+02	.3616437E-01	.1278604E-01
221	8	10	.1380560E+02	.2896625E-01	.9159934E-02
225	1	6	.1100733E+02	.1457937E-01	.5952004E-02
225	2	6	.1126550E+02	.1434976E-01	.5858266E-02
225	3	8	.1195775E+02	.2774777E-01	.9810320E-02
225	4	6	.1222483E+02	.2630215E-01	.1073781E-01
225	5	7	.1284000E+02	.2096930E-01	.7925649E-02
225	6	6	.1305450E+02	.2690580E-01	.1098425E-01
225	7	8	.1358150E+02	.2147081E-01	.7591077E-02
225	8	8	.1380762E+02	.1299946E-01	.4596004E-02
229	1	3	.1101667E+02	.2003886E-01	.1156944E-01
229	2	4	.1125375E+02	.4865908E-01	.2432954E-01
229	3	6	.1195567E+02	.2242501E-01	.9154974E-02
229	4	9	.1219056E+02	.4202406E-01	.1400802E-01
229	5	9	.1282622E+02	.1045390E-01	.3484634E-02
229	6	12	.1306258E+02	.3208445E-01	.9261985E-02
229	7	9	.1356400E+02	.1335841E-01	.4452802E-02
229	8	8	.1377637E+02	.4185682E-01	.1479862E-01

Table B.3: Peak Means and Standard Deviations

YRDAY	RAY #	NUMBER OF DATA	AVG. TIME (S)	STANDARD DEVIATION (S)	MEAN STANDARD DEVIATION (S)
213	1	5	.1105800E+02	.1802216E-01	.8059755E-02
213	2	7	.1130786E+02	.2572620E-01	.9723590E-02
213	3	7	.1201686E+02	.1730776E-01	.6541718E-02
213	4	8	.1227325E+02	.2449362E-01	.8659803E-02
213	5	7	.1288943E+02	.3871459E-01	.1463274E-01
213	6	8	.1310787E+02	.4390460E-01	.1552262E-01
213	7	7	.1362186E+02	.2440396E-01	.9223829E-02
213	8	5	.1383800E+02	.2394151E-01	.1070697E-01
217	1	5	.1106600E+02	.1019820E-01	.4560774E-02
217	2	6	.1131867E+02	.1937057E-01	.7908001E-02
217	3	6	.1202317E+02	.1975206E-01	.8063747E-02
217	4	5	.1227860E+02	.2452434E-01	.1096762E-01
217	5	8	.1288362E+02	.2853480E-01	.1008858E-01
217	6	7	.1307971E+02	.2715423E-01	.1026333E-01
217	7	6	.1360250E+02	.1161540E-01	.4741968E-02
217	8	6	.1382483E+02	.1201946E-01	.4906926E-02
221	1	9	.1103811E+02	.1403538E-01	.4678459E-02
221	2	10	.1128160E+02	.3073500E-01	.9719262E-02
221	3	9	.1199156E+02	.3005962E-01	.1001987E-01
221	4	11	.1224609E+02	.1788062E-01	.5391211E-02
221	5	8	.1283638E+02	.3229141E-01	.1141674E-01
221	6	9	.1309033E+02	.2386558E-01	.7955195E-02
221	7	8	.1357350E+02	.3477056E-01	.1229325E-01
221	8	10	.1380470E+02	.2675831E-01	.8461723E-02
225	1	6	.1100500E+02	.1329172E-01	.5426320E-02
225	2	6	.1126667E+02	.1387644E-01	.5665034E-02
225	3	8	.1195150E+02	.2876630E-01	.1017042E-01
225	4	6	.1222267E+02	.3127135E-01	.1276648E-01
225	5	7	.1283929E+02	.1973917E-01	.7460704E-02
225	6	6	.1305717E+02	.1628318E-01	.6647579E-02
225	7	8	.1358700E+02	.2028546E-01	.7171993E-02
225	8	8	.1381025E+02	.1335817E-01	.4722827E-02
229	1	3	.1100233E+02	.4027969E-02	.2325549E-02
229	2	4	.1125100E+02	.4903077E-01	.2451539E-01
229	3	6	.1195717E+02	.2308982E-01	.9426382E-02
229	4	9	.1219722E+02	.3415251E-01	.1138417E-01
229	5	9	.1282167E+02	.1804918E-01	.6016394E-02
229	6	12	.1306358E+02	.3148407E-01	.9088671E-02
229	7	9	.1356478E+02	.1559771E-01	.5199237E-02
229	8	8	.1377675E+02	.4357379E-01	.1540566E-01

Table B.4: Centroid Means and Standard Deviations

YRDAY	RAY #	NUMBER OF DATA	AVG. TIME (S)	STANDARD DEVIATION (S)	MEAN STANDARD DEVIATION (S)
213	1	5	-.1400000E-02	.6343502E-02	.2836901E-02
213	2	7	.3714286E-02	.1597958E-01	.6039714E-02
213	3	7	.1142857E-02	.4940464E-02	.1867320E-02
213	4	8	.1249997E-03	.1650331E-01	.5834803E-02
213	5	7	-.4285715E-02	.2490800E-02	.9414338E-03
213	6	8	.2500001E-03	.1531952E-01	.5416269E-02
213	7	7	.3000000E-02	.1511858E-02	.5714286E-03
213	8	5	-.3999999E-03	.4586938E-02	.2051341E-02
217	1	5	-.4400000E-02	.1059434E-01	.4737934E-02
217	2	6	-.2333333E-02	.2624670E-02	.1071517E-02
217	3	6	-.6333333E-02	.1278889E-01	.5221042E-02
217	4	5	-.1200000E-02	.4069398E-02	.1819890E-02
217	5	8	-.2500000E-03	.3699663E-02	.1308029E-02
217	6	7	-.5000000E-02	.1109698E-01	.4194264E-02
217	7	6	.4000000E-02	.1690168E-01	.6900082E-02
217	8	6	-.1666666E-03	.4669643E-02	.1906374E-02
221	1	9	-.7777777E-03	.3705185E-02	.1235062E-02
221	2	10	-.3600000E-02	.6311893E-02	.1995996E-02
221	3	9	-.4555555E-02	.8744668E-02	.2914890E-02
221	4	11	-.2454545E-02	.4599677E-02	.1386855E-02
221	5	8	.3125000E-02	.1044555E-01	.3693058E-02
221	6	9	.3880511E-10	.3915782E-02	.1305261E-02
221	7	8	.5375000E-02	.8092245E-02	.2861041E-02
221	8	10	.9000000E-03	.9417538E-02	.2978087E-02
225	1	6	.2333333E-02	.3299833E-02	.1347151E-02
225	2	6	-.1166667E-02	.3890872E-02	.1588442E-02
225	3	8	.6250000E-02	.1503953E-01	.5317279E-02
225	4	6	.2166666E-02	.1473564E-01	.6015799E-02
225	5	7	.7142857E-03	.3057276E-02	.1155542E-02
225	6	6	-.2666667E-02	.2333571E-01	.9526766E-02
225	7	8	-.5500000E-02	.1013657E-01	.3583819E-02
225	8	8	-.2625000E-02	.3870966E-02	.1368593E-02
229	1	3	.1433333E-01	.1602776E-01	.9253630E-02
229	2	4	.2750000E-02	.3561953E-02	.1780976E-02
229	3	6	-.1500000E-02	.3403430E-02	.1389445E-02
229	4	9	-.6666667E-02	.1235584E-01	.4118613E-02
229	5	9	.4555555E-02	.1340905E-01	.4469683E-02
229	6	12	-.1000000E-02	.2581989E-02	.7453561E-03
229	7	9	-.7777778E-03	.3614102E-02	.1204701E-02
229	8	8	-.3750000E-03	.4498264E-02	.1590377E-02

Table B.5: Peak – Centroid Means and Standard Deviations

Bibliography

[1] Barnett, T.P., 1990: Beware Greenhouse Confusion. *Nature*, **343**, 696–697.

[2] Bradley, R.S., H.F. Diaz, G.N. Kiladis and J.K. Eischeid, 1987: ENSO Signal in Continental Temperature and Precipitation Records. *Nature*, **327**, 497–501.

[3] Bushong, P.J., 1987: Tomographic Measurements of Barotropic Motions. Master's Thesis, Joint Program in Ocean Engineering, Massachusetts Institute of Technology and Woods Hole Oceanographic Institute, 48pp.

[4] Clay, C.S. and H. Medwin, 1977: Acoustical Oceanography: Principles and Applications. John Wiley & Sons, New York, 544pp.

[5] Cornuelle, B., R. Heinmiller, R. Knox, K. Metzger, W. Munk, J. Spiesberger, R. Spindell, D. Webb, P. Worcester and C. Wunsch, 1982: A Demonstration of Ocean Acoustic Tomography. *Nature*, **299**, 121–125.

[6] —, 1985: Tomographic Maps of the Ocean Mesoscale. Part 1: Pure Acoustics. *J. Phys. Ocean.*, **15**, 133–152.

[7] Emery, W.J. and K. Hamilton, 1985: Atmospheric Forcing of Interannual Variability in the Northeast Pacific Ocean: Connections With El Niño. *J. Geophys. Res.*, **90**, 857–868.

[8] Enfield, D.B., 1989: El Niño, Past and Present. *Rev. Geophys.*, **27**, 159–187.

[9] Ewing, M. and J.L. Worzell, 1948 in Propagation of Sound in the Ocean, Memoir 27, Part III. The Geological Society of America, New York, 35pp.

[10] Gill, A.E., 1982: Atmosphere-Ocean Dynamics. Academic Press, Inc., New York, 662pp.

[11] Hanawa, K. and H. Yoritaka, 1987: Detection of Systematic Errors in XBT Data and Their Collection. *J. Ocean. Soc. Japan*, **43**, 68–76.

[12] Howe, B.M., P.F. Worcester and R.C. Spindel, 1987: Ocean Acoustic Tomography: Mesoscale Velocity. *J. Geophys. Res.*, **92**, 3785–3805.

[13] Johnson, M.A. and J.J. O'Brien, 1990: The Northeast Pacific Response to the 1982–1983 El Niño. *J. Geophys. Res.*, **95**, 7155–7166.

[14] Kerr, R.A., 1988: La Niña's Big Chill Replaces El Niño. *Science*, **241**, 1037–1038.

[15] Metzger, K., 1983: Signal Processing Equipment and Techniques for Use in Measuring Ocean Acoustic Multipath Structures. Ph. D. Thesis, University of Michigan, 305pp.

[16] Monastersky, R., 1990: Hints of El Niño Surface in Pacific Ocean. *Science News*, **137**, 135.

[17] Munk, W.H. and C. Wunsch, 1979: Ocean Acoustic Tomography: A Scheme for Large Scale Monitoring. *Deep-Sea Res.*, **26A**, 123–161.

[18] *Oceanographic Monthly Summary*, 1987–1989. National Weather Service, National Environmental Satellite, Data, and Information Service and the National Ocean Service, Camp Springs, Maryland.

[19] Philander, S.G., 1990. El Niño, La Niña, and the Southern Oscillation. Academic Press, Inc., San Diego, 293pp.

[20] Pickard, G.L. and W.J. Emery, 1982. Descriptive Physical Oceanography. Pergamon Press, New York, 248pp.

[21] Quinn, W.H., V.T. Neal and S.E. Antunez De Mayolo, 1987: El Niño Occurrences Over the Past Four and a Half Centuries. *J. Geophys. Res.*, **92**, 14,449–14,461.

[22] Reynolds, R.W., 1988: A Real-Time Global Sea Surface Temperature Analysis. *J. of Climate*, **1**, 75–86.

[23] Spiesberger, J.L., T.G. Birdsall, K. Metzger, R.A. Knox, C.W. Spofford, R.C. Spindel, 1983: Measurements of Gulf Stream Meandering and Evidence of Seasonal Thermocline Development Using Long-Range Acoustic Transmissions. *J. Phys. Ocean.*, **13**, 1836–1846.

[24] —, P.J. Bushong, K. Metzger and T.G. Birdsall, 1989: Basin-Scale Tomography: Synoptic Measurements of a 4000 km Length Section in the Pacific. *J. Phys. Ocean.*, **19**, 1073–1090.

[25] — and K. Metzger, 1990a: Basin-Scale Tomography: A New Tool for Studying Weather and Climate. Submitted to *J. Geophys. Res.*.

[26] —, K. Metzger and J.A. Furgerson, 1990b: Acoustic Tomography of Oceans: A New Tool for Studying Weather and Global Warming. Submitted to *Nature*.

[27] —, R.C. Spindel and K. Metzger, 1980: Stability and Identification of Ocean Acoustic Multipaths. *J. Acoust. Soc. Am.*, **67**, 2011–2017.

[28] Stouffer, R.J., S. Manabe and K. Bryan, 1989: Interhemispheric Asymmetry in Climate Response to a Gradual Increase of Atmospheric CO_2. *Nature*, **342**, 660–662.

[29] Trenberth, K.E., 1989: The Wayward Winds. *Natural History*, Jan. 89, 44–45.

[30] —, G.W. Branstator and P.A. Arkin, 1988: Origins of the 1988 North American Drought. *Science*, **242**, 1640–1645.

[31] Vonder Haar, T.H. and A.H. Oort, 1973: New Estimate of Annual Poleward Energy Transport by Northern Hemisphere Oceans. *J. Phys. Ocean.*, **3**, 169–172.

[32] Wyrtki, K. and L. Uhrich, 1982: On the Accuracy of Heat Storage Computations. *J. Phys. Ocean.*, **12**, 1411–1416.

Thesis
F945
c.1

Furgerson
Inter-annual variability of acoustic ray travel times in the Northeast Pacific.